Mucha, Philipp; el Moctar, Ould; Dettmann, Thorsten; Tenzer, Matthias

An experimental study on the effect of confined water on resistance and propulsion of an inland waterway ship

Ocean Engineering

Erstveröffentlichung in Ocean Engineering 167 (2018), S. 11-22.
Verfügbar unter https://doi.org/10.1016/j.oceaneng.2018.08.009

An experimental study on the effect of confined water on resistance and propulsion of an inland waterway ship

Philipp Mucha[a], Ould el Moctar[b], Thorsten Dettmann[a], Matthias Tenzer[c]

[a] Federal Waterways Engineering and Research Institute (BAW), Germany
[b] University of Duisburg-Essen, Germany
[c] Development Centre for Ship Technology and Transport Systems (DST), Duisburg, Germany

Abstract: We present an experimental study on resistance and propulsion characteristics of an inland waterway ship in confined water. Physical experiments of resistance and propulsion with an inland waterway ship were performed. The effects of water depth, separation distance to a vertical wall (bank effects) and forward speed are discussed. The objective of the investigation was to generate benchmark data for validation of Computational Fluid Dynamics (CFD) solvers.

Keywords: Inland waterway ship, Shallow water, Resistance, Propulsion, Bank effects, Model test, Benchmark data for CFD,

1 Introduction

The present study ties in with the investigation of the benchmark test case of a typical inland waterway ship as encountered in European inland shipping, for which geometry and conditions, resistance and propulsion characteristics for a given shallow water condition are publicly available, BAW (2017) and Mucha et al. (2017). The increasing application of Computational Fluid Dynamics (CFD) to predictions of flows around ships in shallow and confined waters and the increasing importance of ship handling simulations for navigability analyses motivated the extension of above test case to include the effect of water depth and separation distance to a vertical wall. These induce powerful hydrodynamic interactions in confined water, and computational predictions require suitable benchmark data for verification and validation. Model tests were planned in collaboration with and conducted by the Development Centre for Ship Technology and Transport Systems (DST) in Duisburg, Germany. The paper is organized as follows. Following the address of relevant references in the field, the test case is introduced in terms of the geometry of the hull, propellers and appendices and the experimental setup. Then, results of resistance, propulsion and near-wall tests are discussed regarding above mentioned sensitivities.

Tuck (1978) is a comprehensive treatise of ship hydrodynamic problems in restricted waters addressing the physical phenomenology of hydrodynamic interactions between ships and flow restrictions. The shallow water effect on the resistance of a slender ship was studied by Graff et al. (1964) by experimental analysis. Ship waves in shallow water were addressed by Chen (1999) and

Jiang (2003). Manoeuvrability analyses of ships in shallow water were presented by Eloot et al. (2015) and Tonelli and Quadvlieg (2015). Gronarz (1997) and Mucha (2017) focused on the mathematical modelling of manoeuvring in shallow water. Validation studies on computational methods for the prediction of resistance and squat are found in Deng et al. (2014) and Mucha et al. (2015, 2016). Terziev et al., 2018 present another effort to assess the capabilities of numerical methods to model ship hydrodynamics in shallow water. Lataire and Vantorre (2008) conducted a systematic investigation of the influence of bank geometry on hydrodynamic interactions between ships and banks. These were investigated with respect to suitable auto-pilots by Thomas and Sclavounos (2006). Measurements of squat and bank effects for a similar, albeit smaller inland waterway ship were presented by Eloot et al. (2012). Vantorre et al. (2002) represents a relevant reference with respect to experimental analysis of ship-ship interactions.

1.1 Shallow water effect on resistance

Hydrodynamic interactions in shallow water can be characterized in terms of water-depth dependent changes in the pressure field ambient to the ship. These effects can be related to the principles mass and energy conservation along a streamline in ideal flow, postulated by the Bernoulli equation. According to the Bernoulli and continuity equation a decrease of the flow cross-section results in a concurrent increase of the flow velocity and a decrease of pressure. Consequences of Bernoulli's effect for floating bodies are dynamic changes of the floating position and orientation. Ships in forward motion experience a vertical displacement in the heave mode (sinkage) and a rotational displacement in the pitch mode (trim) of motion, accompanied by a decrease of the mean ambient water level, decreasing under-keel clearance (UKC), Fig. 1. Owing to the importance of both water depth H and forward speed V_M ,[1] the Depth Froude number $F_{rh} = V_M / \sqrt{gH}$ was established, where g is gravitational acceleration constant. Resistance R_{TM} is affected by above phenomenon by the increase of the dominant contributions defined in the classic decomposition, i.e. friction resistance, viscous pressure resistance and wave resistance, where the total resistance coefficient c_{TM} is defined as

$$c_{TM} = \frac{R_{TM}}{0.5\rho V_M^2 S_M} \qquad (1)$$

where ρ is density of water and S_M the wetted surface of the model. The established decomposition of c_{TM} is

$$c_{TM} = c_F(1 + k) + c_W + c_A + c_{AA} \qquad (2)$$

where c_F is friction resistance coefficient as in Eq. (3), k form factor, c_W wave resistance coefficient, c_A and c_{AA} are correlation allowance and air resistance coefficients, respectively, ITTC (1999). At higher speeds $V_M > \sqrt{gH}$ the effect of the change in floating position on wave resistance is dominant. Extrapolation procedures for model results to full-scale dimensions, e.g. applying the ITTC 1978

performance prediction method, are considered questionable with regard to the friction resistance coefficient c_F

$$c_F = \frac{0.075}{(\log_{10} Re - 2)^2} \qquad (3)$$

and the form factor k, ITTC (1999), which is determined through regression analysis of measurements. Reynolds number is $R_e = V_M L_{PP}/\nu$. Above mentioned approach does not consider the influence of limited UKC and was established for deep water.

1.2 Shallow water effect on propulsion

The limited UKC might significantly affect propulsion performance. In shallow water the flow field in the propeller plane changes in response to a higher wake with more distinct flow separation and interactions of the flow field ambient to the hull with the tank, canal bottom or seabed, respectively. Thus, to attain the same forward speed as when sailing in deep water, more power has to be delivered. The operating propeller decreases the local pressure on the after body compared to an equivalent flow in bare hull condition or with the propeller not in operation, which gives rise to a bow-up moment about the transverse axis with increasing forward speed. The flow field in the propeller plane in shallow water condition is usually characterized by a widening of isolines of the ratio of longitudinal flow velocity component to flow velocity of the undisturbed flow u_x/u_0, smaller local wake numbers quantified by u_x/u_0 and interaction with the vertical flow restriction. A related CFD analysis based on the solution of Reynolds-averaged Navier-Stokes (RANS) equations was performed by Mucha (2017) to demonstrate the qualitative effects. Fig. 2 shows scalar plots of u_x/u_0 in the propeller plane of the Kriso Containership (KCS) at different water depth to draft ratios H/T.

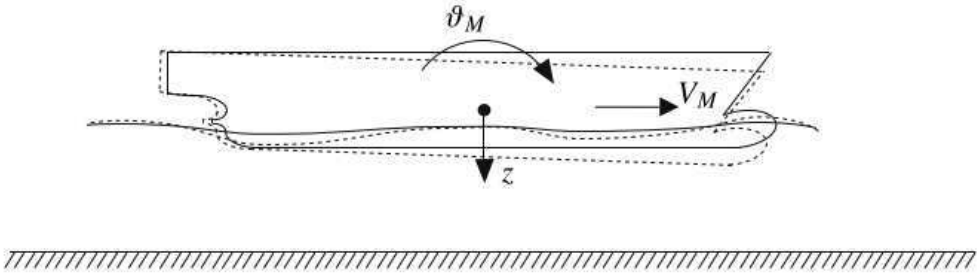

Figure 1: Schematic of a ship underway experiencing bow-down squat. Dashed lines indicate the orientation of the ship and shape of the ambient water level caused by squat.

1.3 Ship-bank interactions

Analogous interactions occur in horizontal modes of motion in laterally confined water. Forces and moments arising from pressure variations on the ship hull, when traveling at close separation distance to a wall or bank, came to be denoted by the term bank effects. The decreased flow cross-section results in a decrease of pressure on the side of the restriction, inducing a suction force towards the wall and a moment, which for most conventional ship hulls tends to turn the ship bow-out off the

wall. Lateral forces on the fore and after body strongly depend on UKC, distance to the restriction and forward speed and, in some cases, might result in an integral force which is repulsive, Lataire (2014). A change in ambient water level accompanies the suction effects, and at high speeds, the difference between the water levels on the open water side and the side facing the restriction dominates the suction forces and increases proportionally to the difference in water level. Fig. 3 is a schematic of a typical ship-bank interaction scenario. The suction force and bow-out moment cause the ship to move closer to the wall and induce a Munk moment. Typically, applying rudder in the direction of the wall while still maintaining a small bow-out drift mitigates the bank effects. In shallow water, bank effects are more pronounced as the blockage of the flow reinforces the change of the pressure field.

2 Test case description

The inland waterway ship used in the present investigation was designed in cooperation with DST and can be used for various ship types, e.g. for a tanker, bulk carrier and container ship, DST report 2112 (2014). No full-scale representation exists. The model is equipped with two ducted propellers and can be configured with single or twin rudders, i.e. a pair of rudders for each propeller. The rudders feature a fishtail and a small geometric aspect ratio of $\Lambda_R = 0.983$, typical for inland waterways ships. Table 1 summarizes the main particulars for the design loading condition, Fig. 4 shows a lines plan and Table 2 describes the appendages geometry. Computational Aided Design (CAD) files are publicly available, BAW (2017). Mucha et al. (2017) provides a comprehensive description of the hull and appendages geometries. A righthanded Cartesian coordinate system $\mathscr{S}$ participating in the forward motion of the model is used, Fig. 5. The origin is located at the midship section, in the centre and calm waterline plane, where x, y, z point forward, to starboard and downward, respectively. Longitudinal measured force is X and equals the negative ship resistance. Trim angle ϑ_M is positive bow-up. The distance between the centreline of the ship and the tank wall is denoted by d, Fig. 6. Midship sinkage is z_{VM}, sinkage at the fore measurement point z_{VF} and at the aft measurement point z_{VA}. Trim angle ϑ_M is given in minutes of arc.

Resistance tests were performed in bare hull condition at three water depths corresponding to H/T of 2.0, 1.5 and 1.2 in the shallow water tank of DST (dimension of the towing tank: 200 m long, 10 m wide, 0–1.1 m deep). Besides, results of towing tests in the deep water tank of the Schiffbauversuchsanstalt (SVA) Potsdam are available. The model was free to heave and pitch, but otherwise constrained. During tests in proximity to the tank wall the model was allowed to roll and the

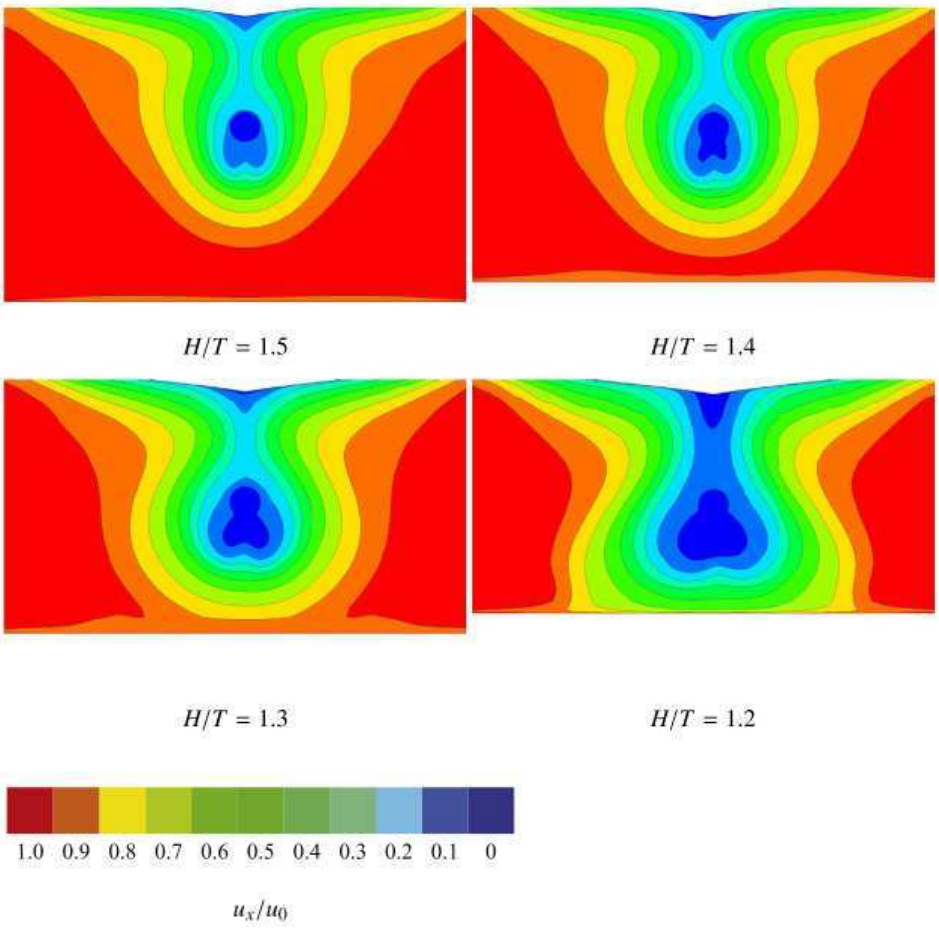

Figure 2: Nominal wake distribution of KCS model with respect to UKC, H/T = 1.2, 1.3, 1.4 and 1.5.

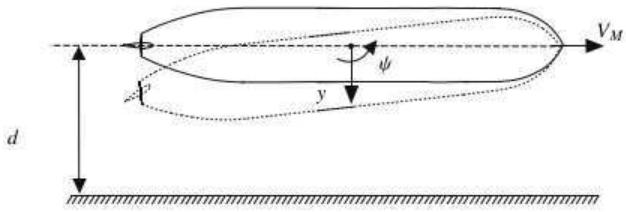

Figure 3: Schematic of bank effects acting on a ship underway. Dashed line represent a typical orientation of a ship to mitigate lateral suction force and a bow-out moment.

Table 1: Main particulars of the ship at rest and zero static trim.

	Symbol	Model	Ship
Length of waterline [m]	L_{WL}	8.4013	134.42
Length between perpendiculars [m]	L_{PP}	8.4375	135.00
Waterline breadth [m]	B_{WL}	0.7150	11.45
Overall breadth [m]	B	0.7150	11.45
Mean draught [m]	T_m	0.2188	3.5
Wetted surface area [m^2]	S	9.2817	2376.1
Displacement [m^3]	V	1.2187	4992
Longitudinal centre of gravity [m]	x_{CG}	−0.01074	−0.1718
Block coefficient [-]	C_B	0.92	0.92

heel angle was measured. Turbulence stimulating struts were installed at distances 0.4211 m and 0.4236 m aft of the bow. Water temperature was 18.4 °C (ρ = 998.52 kg/m^3, kinematic viscosity ν = $1.04 \cdot 10^{-6}$m^2/s). Forces on the model were measured using electronic gauges. At DST sinkage was measured by way of laser at positions 2.803 m astern and 2.858 m ahead of the midship section. At SVA potentio-metres were applied to measure the sinkage of the model in the fore and aft ship. Tables 3–6 and Figs. 8–9 summarize results of resistance tests. Fig. 7 shows an example of the time series of measurements (low-pass filtered, cut-off frequency 1 Hz). Consistent with the motivation of the present work to provide benchmark data for computational methods and the challenges associated with the extrapolation to full-scale dimensions, only model results as measured are presented. Owing to the increasing blockage of the flow in shallow water and dynamic responses in heave and pitch of the ship model underway, the choice of forward speeds had to be adapted in the shallow water tank at DST.

In order to perform towed model tests in proximity to the tank wall at distance d, DST installed a special beam to the towing carriage to allow for an eccentric guidance of the model. Lateral forces on the model were measured with electronic gauges at positions 1.94 m aft and 1.96 m ahead of the midship section. They are given as Y_a for the force measured at the aft position and as Y_f for the force measured at the fore position. Near-wall resistance tests were conducted at H/T = 1.2.

3 Results

3.1 Resistance

Fig. 8 shows the trends of resistance over forward speed for the water depths under investigation. Results showed the characteristic nonlinear trends of R_T (V_M). According to theory, at lower speeds friction resistance and viscous pressure resistance dominate R_T, while the

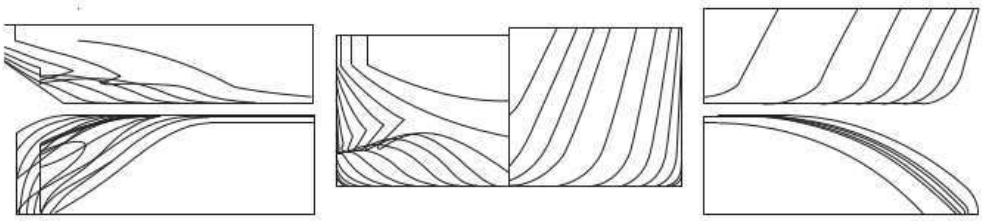

Figure 4: Lines plan of the inland waterway ship (not drawn to scale).

Table 2: Propeller and duct main particulars in model scale. Pitch at 0.7 of the propeller radius is P_{07}, A_E is expanded propeller area, A_0 is propeller disc area.

Scale factor [-]	λ	16
Diameter [m]	D_P	0.1
Chord length [m]	C_{07}	0.04075
Number of blades [-]	Z	4
Pitch ratio [-]	P_{07}/D_P	1.052
Disc ratio [-]	A_E/A_0	0.71
Inner duct diameter [m]	D_i	0.102
Duct length to diameter ratio [-]	L_D/D_i	0.5392
Relative propeller position [-]	x_P/L_D	0.4

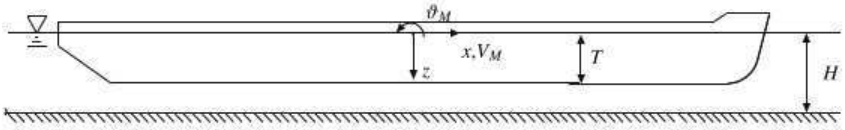

Figure 5: Coordinate system for resistance and propulsion tests.

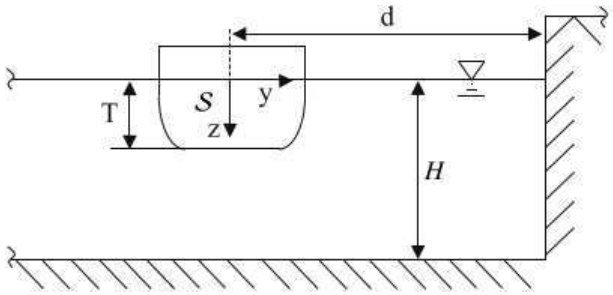

Figure 6: Definition of ship dimensions and associated notation in restricted water.

contribution of wave resistance is increasing to become the greatest in the higher forward speed range. The distance between data points with respect to water depth increases nonlinearly, too. Resistance approximately doubled at the shallowest water condition H/T = 1.2 at V_M = 0.97 m/s compared to deep water.

The comparison between results from resistance experiments at H/T = 1.2, which were performed in the middle of the tank (equivalent to d/L = 0.6), to those performed eccentrically at distances d/L = 0.3, d/L = 0.2 and d/L = 0.1 reveal that the lateral restriction of the flow leads to a further increase of resistances, quantified in Tables 7, 9 and 11. At lower carriage speeds the effect is moderate, but becomes notable for higher speeds and the smallest separation distance d/L = 0.1. In theory, the

altered pressure fields at both stagnation points and ambient to the parallel midship section, both of which take distinct asymmetric shapes with respect to the ship centre-line, affect viscous resistance contributions more at lower forward speeds. At higher speeds wave resistance becomes dominant again, in this case the asymmetric flow results in significantly higher free surface elevation and depression in above mentioned areas around the ship on the side facing the wall.

Fig. 9 presents the results for squat in terms of the trends of midship sinkage z_{VM} and trim angle ϑ_M over carriage speed. The characteristic nonlinear trends of both quantities were observed over both speed and water depth. The difference of results regarding the variation of water depth is more pronounced than for resistance, e.g. when comparing

Table 3: Results of resistance tests at SVA, $H/T = \infty$

V_M [m/s]	Fr [-]	Fr_h [-]	$Re \cdot 10^{-6}$ [-]	R_{TM} [N]	$c_{TM} \cdot 10^{-3}$ [-]	z_{VM}[mm]	ϑ_M [1/60°]
0.556	0.061	–	4.295	6.36	4.458	1.7	-0.18
0.694	0.076	–	5.369	9.65	4.328	2.0	-0.3
0.833	0.092	–	6.443	13.59	4.230	2.4	-0.6
0.972	0.107	–	7.517	18.24	4.172	3.0	-0.84
1.250	0.138	–	9.664	31.20	4.317	4.6	-1.56

Table 4: Results of resistance tests at DST, $H/T = 2.0$

V_M [m/s]	Fr [-]	Fr_h [-]	$Re \cdot 10^{-6}$ [-]	R_{TM} [N]	$c_{TM} \cdot 10^{-3}$ [-]	z_{VM}[mm]	ϑ_M [1/60°]
0.974	0.107	0.470	7.84	20.34	4.73	7.7	-1.52
1.114	0.123	0.538	8.97	27.21	4.84	11.5	-1.93
1.224	0.135	0.591	9.85	35.16	5.18	15.9	-2.48
1.328	0.146	0.641	10.70	45.89	5.74	19.3	-3.39

respective results to the $H/T = 2.0$ and $H/T = 1.5$ condition. Drawing

Table 5: Results of resistance tests at DST, $H/T = 1.5$

V_M [m/s]	Fr [-]	Fr_h [-]	$Re \cdot 10^{-6}$ [-]	R_{TM} [N]	$c_{TM} \cdot 10^{-3}$ [-]	z_{VM}[mm]	ϑ_M [1/60°]
0.904	0.1	0.504	7.28	19.78	6.03	9.3	-1.69
0.974	0.107	0.543	7.4	22.96	5.91	11.5	-2.06
1.048	0.115	0.584	8.44	28.10	6.54	15.4	-2.51
1.114	0.123	0.621	8.97	33.97	6.63	19.3	-3.0

Table 6: Results of resistance tests at DST, $H/T = 1.2$

V_M [m/s]	Fr [-]	Fr_h [-]	$Re \cdot 10^{-6}$ [-]	R_{TM} [N]	$c_{TM} \cdot 10^{-3}$ [-]	z_{VM}[mm]	ϑ_M [1/60°]
0.765	0.084	0.477	6.16	18.30	6.90	5.5	-2.01
0.834	0.092	0.522	6.71	21.93	6.95	11.3	-2.77
0.974	0.107	0.607	7.84	35.06	8.15	18.4	-5.06
1.048	0.225	0.653	8.44	53.05	10.07	26.1	-7.93

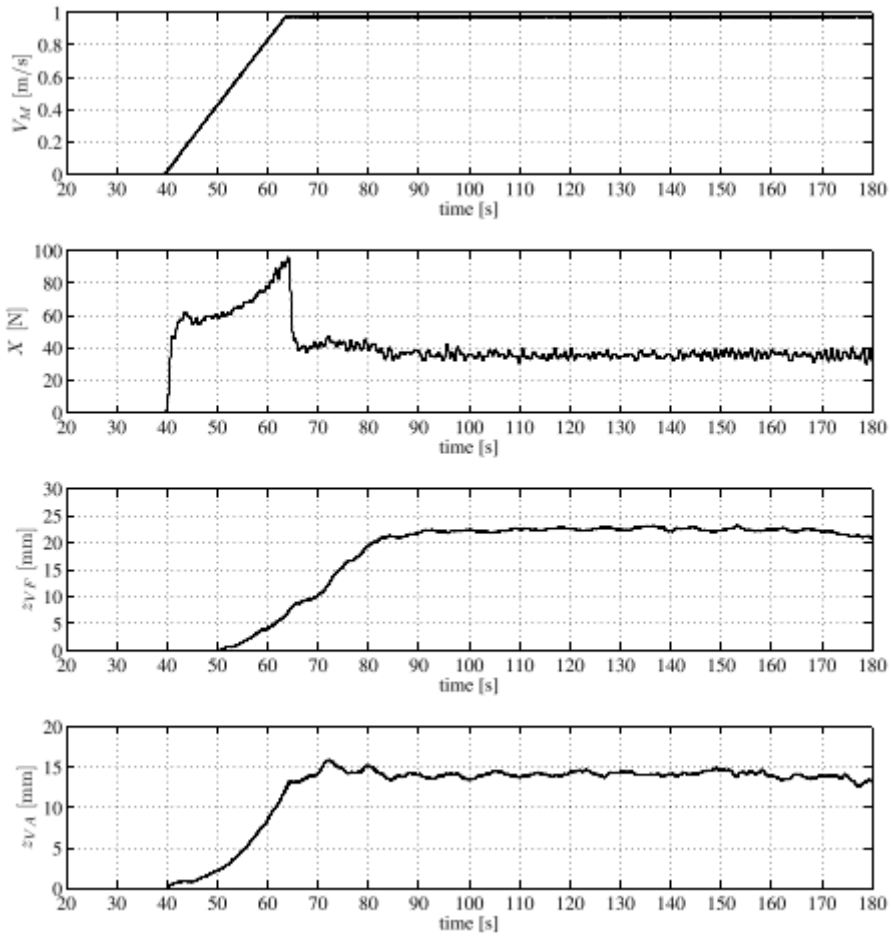

Figure 7: Exemplary time histories of measured longitudinal force during a resistance test run, V_M = 0.974 m/s at H/T = 1.2, Mucha et al. (2017).

the comparison between the deep water and the shallowest water condition around V_M = 0.97 m/s, both midship sinkage and bow-down trim increased by factor six.

When underway at H/T = 1.2 in proximity to a vertical wall, squat increases compared to being towed in the middle of the tank because of higher blockage of the flow. However, the increase becomes notable for midship sinkage only at the two closest distances to the wall; trim increased significantly only at the closest distance d/L = 0.1, Fig. 10. The change of trim characteristic in terms of a decrease of the bow-down trim at the highest forward speed at d/L = 0.1 is notable. Theoretically, it could be associated with the modified wave pattern in the bow area.

Repetitions of test runs are desirable to confirm this notion. Results comprise measurements of the heel angle φ, which can become relevant in light of the asymmetry of the flow around the model due to the wall on the starboard side. According to measurements, φ increases with increasing speed and decreasing separation distance to the wall, albeit its magnitude is altogether small. At the highest speed and closest distance to the wall, the model heels φ = 0.86∘ to the side of the wall. In terms of the non-dimensional sinkage as a percentage of the gross UKC similar magnitudes were obtained

with the present test case compared to squat measurements with an inland waterway ship model of smaller length (L = 110 m), Eloot et al. (2012). At H/T = 1.2 and $F_r \approx 0.12$ this

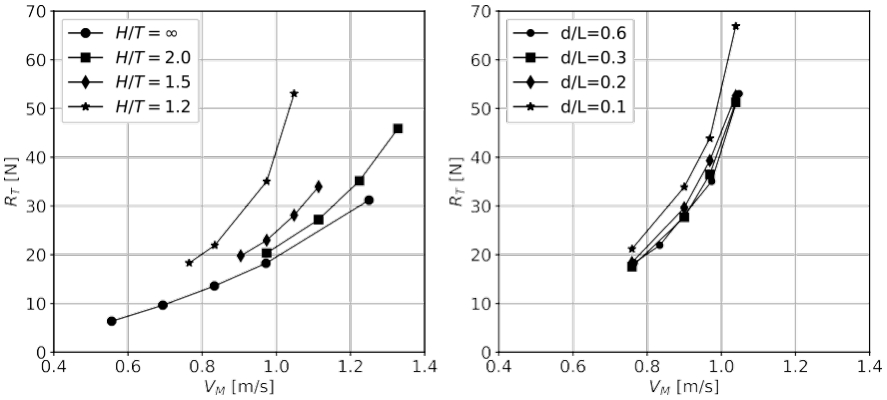

Figure 8: Resistance test results over forward speed at different water depths (left) and over forward speed at different wall distances at fixed water depth H/T = 1.2 (right).

Table 7: Results of resistance tests at DST, d/L = 0.3, H/T = 1.2.

V_M [m/s]	Fr [-]	Fr_h [-]	$Re \cdot 10^{-6}$ [-]	R_{TM} [N]	$c_{TM} \cdot 10^{-3}$ [-]	z_{VM} [mm]	ϑ_M [1/60°]	φ [°]
0.759	0.084	0.474	6.19	17.55	6.71	8.5	-1.94	0.016
0.900	0.099	0.561	7.33	27.69	7.55	15.0	-3.36	0.013
0.969	0.107	0.605	7.90	36.48	8.56	18.6	-5.20	-0.019
1.039	0.114	0.648	8.47	51.28	10.05	26.3	-7.44	-0.172

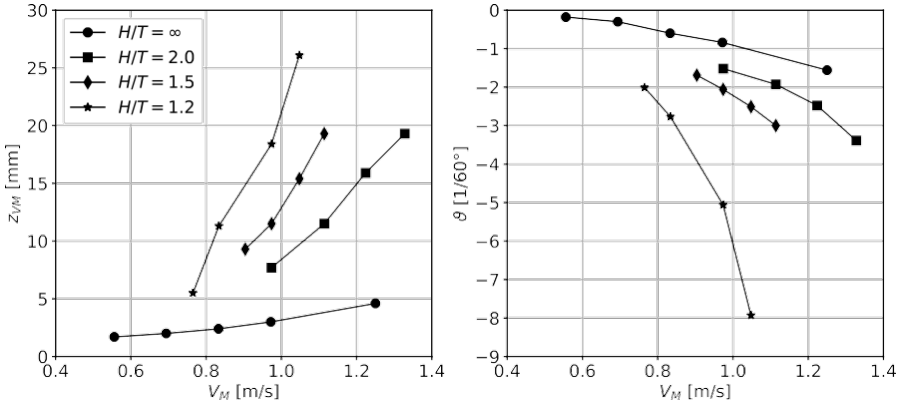

Figure 9: Sinkage (left) and trim angle (right) over forward speed at different water depths.

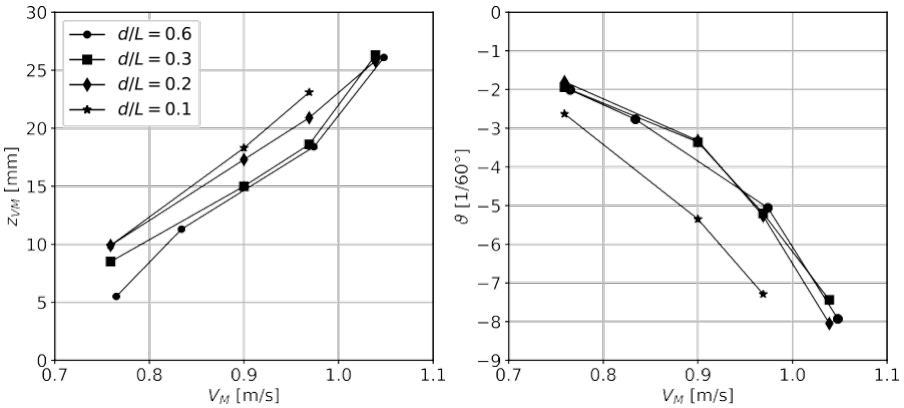

Figure 10: Sinkage (left) and trim angle (right) over forward speed at different wall distances and at fixed water depth H/T = 1.2.

value is between 30 and 40% for both kinds of ships. Moreover, the tendency for trimming bow-down in the sub-critical speed regime was observed for both ship models.

In terms of ship motions in the horizontal plane when sailing in close proximity to lateral restrictions, hydrodynamics in the sway and yaw mode of motion are of particular interest, because of aforementioned bank effects. Lateral forces measured at the fore and aft position are directed to the wall. The force measured in the after body section is

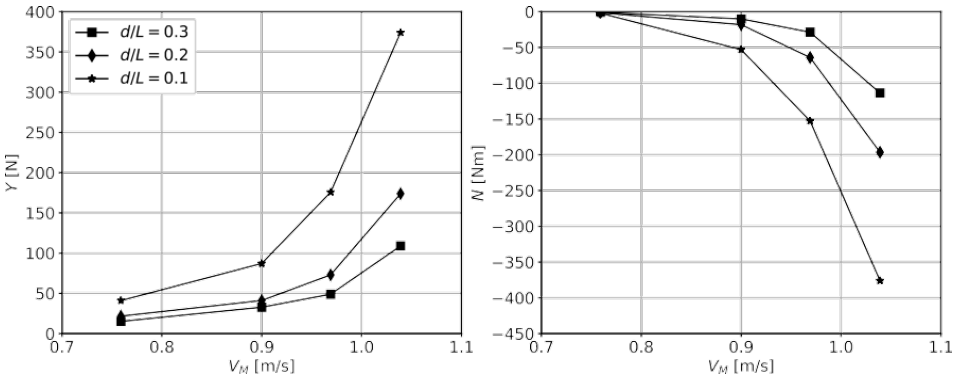

Figure 11: Suction force (left) and bow-out moment (right) over forward speed at different wall distances and fixed water depth H/T = 1.2.

Table 8: Results of resistance tests at DST, suction forces and bow-out yaw moment N, d/L = 0.3, H/T = 1.2

V_M [m/s]	Y_a [N]	Y_f [N]	Y [N]	N [Nm]
0.759	7.84	7.34	15.18	-0.82
0.900	19.05	13.73	32.78	-10.02
0.969	31.96	16.98	48.94	-28.65
1.039	83.97	24.96	108.93	-113.69

Table 9: Results of resistance tests at DST, d/L = 0.2, H/T = 1.2.

V_M [m/s]	Fr [-]	Fr_h [-]	$Re \cdot 10^{-6}$ [-]	R_{TM} [N]	$c_{TM} \cdot 10^{-3}$ [-]	z_{VM} [mm]	ϑ_M [1/60°]	φ [°]
0.759	0.084	0.474	6.19	18.40	7.04	9.9	-1.8	0.018
0.900	0.099	0.561	7.33	29.63	8.07	17.3	-3.32	-0.004
0.969	0.107	0.605	7.91	39.32	9.21	20.9	-5.27	-0.059
1.039	0.114	0.648	8.47	51.60	10.08	25.8	-8.05	-0.370

Table 10: Results of resistance tests at DST, suction forces d/L = 0.2, H/T = 1.2

V_M [m/s]	Y_a [N]	Y_f [N]	Y [N]	N [Nm]
0.759	11.31	10.40	21.71	-1.55
0.900	25.33	15.83	41.16	-18.07
0.969	53.14	19.85	72.99	-64.02
1.039	137.90	35.99	173.89	-196.48

Table 11: Results of resistance tests at DST, d/L = 0.1, H/T = 1.2.

V_M [m/s]	Fr [-]	Fr_h [-]	$Re \cdot 10^{-6}$ [-]	R_{TM} [N]	$c_{TM} \cdot 10^{-3}$ [-]	z_{VM} [mm]	ϑ_M [1/60°]	φ [°]
0.759	0.084	0.474	6.19	21.16	8.10	9.9	-2.63	0.072
0.900	0.099	0.561	7.33	33.88	9.24	18.3	-5.35	0.037
0.969	0.107	0.605	7.91	43.86	10.03	23.1	-7.29	-0.130
1.039	0.114	0.648	8.47	66.92	10.37	26.9	-3.03	-0.860

Table 12: Results of resistance tests at DST, suction forces, d/L = 0.1, H/T = 1.2

V_M [m/s]	Y_a [N]	Y_f [N]	Y [N]	N [Nm]
0.759	21.15	19.91	41.06	-2.00
0.900	57.44	29.72	87.16	-53.04
0.969	127.60	48.18	175.78	-152.71
1.039	284.70	89.46	374.16	-376.00

generally the greatest of these two, giving rise to a bow-out moment. For conventional ship hulls this is the usual condition. The magnitude of forces is strongly dependent on forward speed and separation distance. The integral lateral force approximately tripled when comparing test runs at the highest speed at d/L = 0.3 and, see Fig. 11d/L = 0.1. In such flow regimes the magnitude of the lateral force even exceeds the magnitude of the longitudinal force. In analogy to the discussion of force contributions to resistance, the effect of free-surface effects, namely a difference between the mean water levels on the port and starboard side, are anticipated to be powerful at higher forward speed. Tables 8, 10 and 12 summarize these results.

Table 13: Results of propulsion tests at DST using the British Method, V_M = 0.899 m/s, H/T = 1.2.

n_{STB} [1/s]	n_{PS} [1/s]	F_{res} [N]	T_{STB} [N]	T_{PS} [N]	Q_{STB} [Nm]	Q_{PS} [Nm]
18.367	18.349	-0.366	12.893	12.593	0.144	0.148
18.510	18.495	-0.583	12.985	12.746	0.145	0.151
19.183	19.162	1.619	14.058	13.716	0.157	0.161
19.795	19.768	3.167	15.414	14.717	0.171	0.172

3.2 Propulsion

Propulsion tests were run with two rudders behind each ducted propeller and followed the British Method, ITTC (1999). The model was mounted to the carriage moving with constant forward speed. For each forward speed three or four propeller rates of revolution were set. The residual towing force F_{res} was measured. A cable pull was installed to apply a friction deduction force F_D using weights according to ITTC (1999). Table 13 shows the results of one propulsion test and the procedure of the British Method. Fig. 12 shows the respective time histories of measurements during the test for V_M = 0.899 m/s. The oscillations of the sinkage at the fore measurement point were caused by the

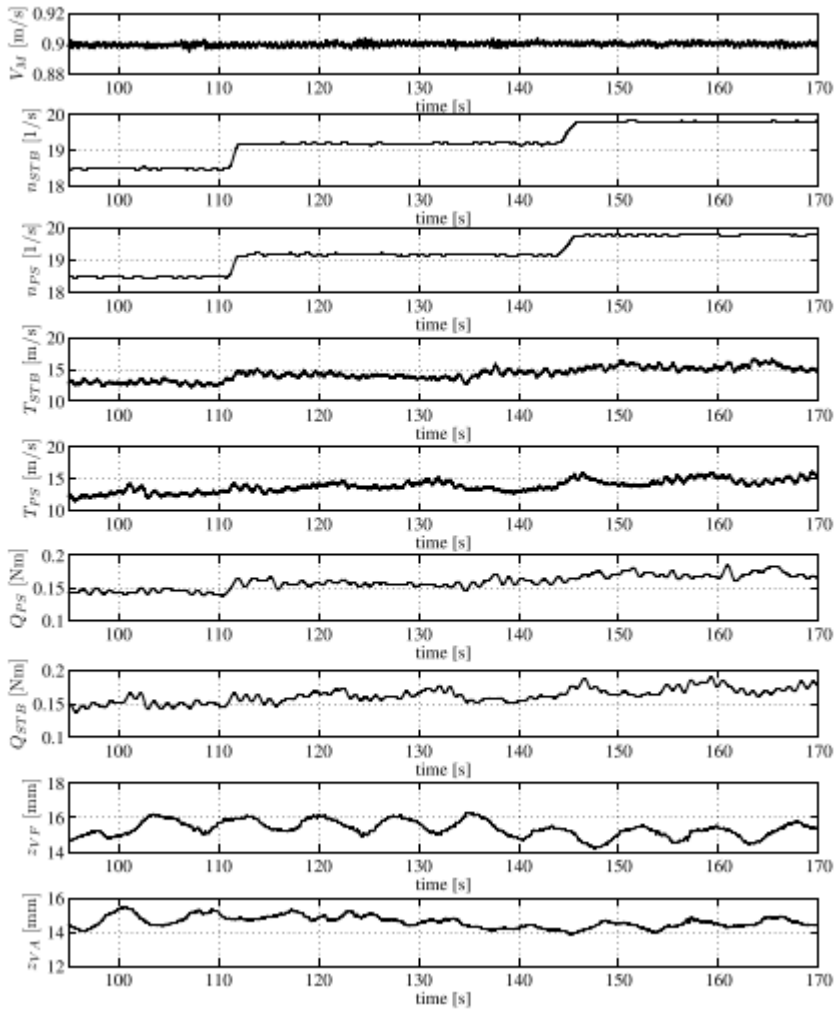

Figure 12: Time histories of propulsion test data, V_M = 0.899 m/s, H/T = 1.2.

Table 14: Open-water propeller characteristics at DST.H/T = 4.57

J [-]	K_{TP} [-]	K_{TD} [-]	K_{TT} [-]	$10K_Q$ [-]	η_0 [-]
0.000	0.2789	0.2464	0.5253	0.4958	0.0000
0.099	0.2712	0.1980	0.4692	0.4819	0.1538
0.200	0.2630	0.1488	0.4118	0.4695	0.2798
0.300	0.2498	0.1077	0.3575	0.4491	0.3809
0.401	0.2317	0.0717	0.3034	0.4221	0.4588
0.497	0.2025	0.0356	0.2382	0.3780	0.4985
0.595	0.1755	0.0101	0.1856	0.3387	0.5194
0.695	0.1320	-0.0278	0.1042	0.2734	0.4216
0.785	0.0861	-0.0640	0.0221	0.2038	0.1356

Table 15: Interpolated results of propulsion tests at DST, H/T = 2.0.

V_M [m/s]	Fr [-]	Fr_h [-]	F_D [N]	P_{DM} [W]	z_{VM} [mm]	ϑ_M [1/60°]
0.759	0.084	0.366	4.20	12.57	4.5	-0.51
0.970	0.107	0.468	6.41	25.24	7.6	-0.91
1.110	0.122	0.536	8.10	41.76	11.7	-1.15
1.215	0.134	0.586	9.49	61.48	15.8	-1.37
1.250	0.138	0.603	9.98	68.06	17.5	-1.46

encounter of reflected waves in the tank which were induced by the acceleration of the model in the beginning of the test. The test run plotted in Fig. 12 was performed after 40 min waiting time with a depth Froude number of F_{rh} = 0.56. The previous test run was at 0.97 m/s corresponding to F_{rh} = 0.6. So there were unavoidable basin residues with an amplitude of less than 0.5 mm present. However, the eigen-period of the basin at this water depth is approximately 4 min. The visible oscillations in Fig. 12 have a period of 8 s and are assigned to transient shallow water effects. Thrust was measured at propellers and ducts on the port and starboard side and the given value includes the force on the ducts. It is denoted by T_T. Thrust generated by each propeller on the starboard and port side is T_{STB} and T_{PS}, respectively. In analogy, Q_{STB} and Q_{PS} denote the respective torques; Q_T is their sum. The arithmetic average of propeller rates of revolution at the self-propulsion point is n_M. Delivered power is P_{DM}. Since the emphasis of the present work is on the provision of benchmark data for comparison with computational methods, the discussion of propulsion tests centers on results of the measurements, rather than on the derivation of propulsion characteristics and efficiency.

Prior to discussing results of propulsion tests, open-water characteristics of the propellers are given. Results refer to tests at DST using n_M = 37 s^{-1} at water depth H =1 m, Table 14. Thrust is T and torque is Q. Non-dimensional thrust coefficient is K_T

Table 16: Results of propulsion tests at DST, H/T = 2.0.

V_M [m/s]	T_{STB} [N]	T_{PS} [N]	T_T [N]	Q_{STB} [Nm]	Q_{PS} [Nm]	Q_T [Nm]	n_{STB} [1/s]	n_{PS} [1/s]	n_M [1/s]
0.759	5.58	6.48	12.06	0.072	0.074	0.15	13.70	13.71	13.71
0.970	8.69	9.87	18.56	0.116	0.116	0.23	17.30	17.33	17.32
1.110	12.38	13.70	26.08	0.164	0.162	0.33	20.37	20.41	20.39
1.215	16.14	16.95	33.08	0.211	0.211	0.42	23.17	23.20	23.19
1.250	17.36	18.73	36.08	0.227	0.225	0.45	23.94	23.99	23.97

Table 17: Interpolated results of propulsion tests at DST, H/T = 1.5.

V_M [m/s]	Fr [-]	Fr_h [-]	F_D [N]	P_{DM} [W]	z_{VM} [mm]	ϑ_M [1/60°]
0.480	0.053	0.267	1.89	3.84	1.8	-0.08
0.690	0.076	0.385	3.50	11.55	4.8	-0.13
0.830	0.091	0.463	4.81	20.61	8.3	-0.21
0.970	0.107	0.541	6.30	36.27	13.2	-0.65
1.040	0.115	0.580	7.12	46.52	15.3	-0.87

$$\eta_0 = \frac{K_T J}{K_Q 2\pi} \qquad (6)$$

where $J = V_M/(n_M D_P)$ is advance coefficient. Propeller thrust coefficient is K_{TP}, duct thrust coefficient is K_{TD} and total thrust coefficient is K_{TT}, found from

$$K_{TT} = K_{TP} + K_{TD} \qquad (7)$$

Tables 15–20 comprise an array of information both from direct measurements and derivation. Measured thrust includes the contribution of the ducts. The transient effects of viscous flow separations is assumed to be the cause for variations of thrust between port and starboard side, where observed in Table 13 and Fig. 12. Detailed flow measurements with time-resolved Particle Image Velocimetry (PIV) technique might provide expanded insight into the phenomenon. Results represent interpolated values. For each water depth investigated, the applied friction deduction force F_D, delivered power P_{DM} and squat are given for each forward speed. A separate table includes propeller rates of revolution n, thrust and torque for both propellers individually and for the propulsion system on aggregate (see Table 21).

Consistent with the increase of resistance in shallow water, more power is required to attain respective forward speeds (Fig. 13), generated by increasing propeller revolutions. Consequently, thrust and torque increase (see Tables 22, 25, 28). According to the experiments, mean sinkage at the fore and aft measurement point hardly change over

Table 18: Results of propulsion tests at DST, H/T = 1.5.

V_M [m/s]	T_{STB} [N]	T_{PS} [N]	T_T [N]	Q_{STB} [Nm]	Q_{PS} [Nm]	Q_T [Nm]	n_{STB} [1/s]	n_{PS} [1/s]	n_M [1/s]
0.480	3.03	3.58	6.61	0.031	0.036	0.07	9.12	9.13	9.13
0.690	5.38	5.97	11.36	0.067	0.072	0.14	13.23	13.22	13.28
0.830	8.04	8.98	17.02	0.100	0.104	0.20	16.08	16.08	16.08
0.970	12.17	13.42	25.59	0.148	0.151	0.30	19.30	19.31	19.31
1.040	14.10	15.26	29.36	0.175	0.177	0.35	21.03	21.04	21.04

Table 19: Interpolated results of propulsion tests at DST, H/T = 1.2.

V_M [m/s]	Fr [-]	Fr_h [-]	F_D [N]	P_{DM} [W]	z_{VM} [mm]	ϑ_M [1/60°]
0.480	0.053	0.299	2.20	9.76	3.40	-0.20
0.690	0.076	0.430	4.10	13.69	7.27	-0.13
0.759	0.084	0.473	4.84	17.30	9.00	-0.17
0.899	0.099	0.560	6.49	35.74	15.10	-0.58
0.970	0.107	0.604	7.40	54.49	21.30	-1.25

Table 20: Results of propulsion tests at DST, H/T = 1.2.

V_M [m/s]	T_{STB} [N]	T_{PS} [N]	T_T [N]	Q_{STB} [Nm]	Q_{PS} [Nm]	Q_T [Nm]	n_{STB} [1/s]	n_{PS} [1/s]	n_M [1/s]
0.480	3.48	4.12	7.6	0.037	0.040	0.077	9.75	9.76	9.76
0.690	6.36	7.49	13.85	0.072	0.075	0.150	13.68	13.69	13.69
0.759	7.82	8.69	16.51	0.090	0.092	0.182	15.12	15.13	15.13
0.899	13.17	13.23	26.40	0.156	0.148	0.340	18.70	18.72	18.71
0.970	17.88	18.28	36.16	0.210	0.201	0.411	21.09	21.11	21.10

Table 21: Results of power, squat and heel measurements from self-propelled tests at DST d/L = 0.3, H/T = 1.2.

V_M [m/s]	Fr [-]	Fr_h [-]	F_D [N]	P_{DM} [W]	z_{VM} [mm]	ϑ_M [1/60°]	φ [°]
0.486	0.053	0.299	0.01	6.34	3.4	-0.02	-0.003
0.694	0.076	0.430	−0.89	13.44	8.00	-0.02	-0.019
0.900	0.099	0.560	−2.28	34.42	16.7	-0.33	-0.029

$$K_T = \frac{T}{\rho n_M^2 D_p^4} \qquad (4)$$

Non-dimensional torque coefficient is K_Q

$$K_Q = \frac{Q}{\rho n_M^2 D_p^5} \tag{5}$$

Propeller open-water efficiency is given by

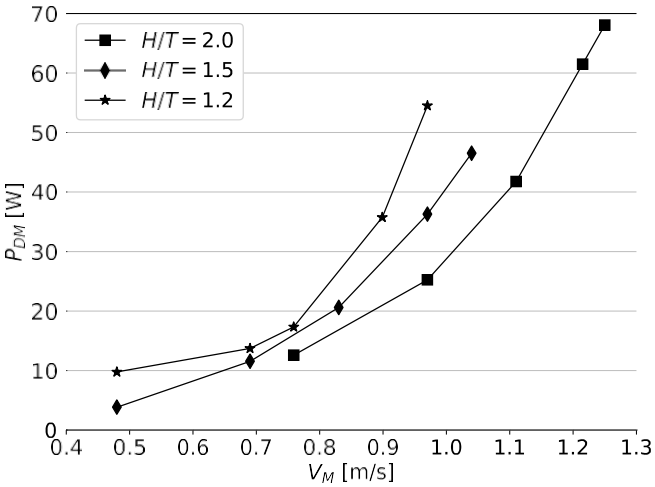

Figure 13: Delivered power over forward speed at different water depths.

Table 22: Results of thrust and torque measurements from self-propelled tests at d/L = 0.3, H/T = 1.2.

V_M [m/s]	T_{STB} [N]	T_{PS} [N]	T_T [N]	Q_{STB} [Nm]	Q_{PS} [Nm]	Q_T [Nm]	n_{STB} [1/s]	n_{PS} [1/s]	n_M [1/s]
0.486	3.70	3.04	6.74	0.057	0.044	0.101	9.71	9.73	9.72
0.694	6.76	6.29	13.05	0.081	0.074	0.155	13.55	13.53	13.54
0.900	13.96	13.15	27.11	0.152	0.142	0.294	18.66	18.67	18.67

Table 23: Results of bank effects measurements from self-propelled tests at DST d/L = 0.3, H/T = 1.2.

V_M [m/s]	Y_a [N]	Y_f [N]	Y [N]	N [Nm]
0.486	1.85	0.86	2.71	-1.89
0.694	9.54	3.15	12.69	-12.30
0.900	17.47	9.27	26.74	-15.69

Table 24: Results of self-propelled tests at DST d/L = 0.2, H/T = 1.2.

V_M [m/s]	Fr [-]	Fr_h [-]	F_D [N]	P_{DM} [W]	z_{VM} [mm]	ϑ_M [1/60°]	φ [°]
0.480	0.053	0.299	-0.57	4.50	3.60	-0.04	-0.013
0.690	0.076	0.430	-2.62	11.78	7.50	0.30	-0.036
0.759	0.076	0.430	-3.51	16.38	10.30	0.27	-0.044
0.900	0.099	0.560	-6.91	32.75	19.50	1.53	-0.064

Table 25: Results of self-propelled tests at DST d/L = 0.2, H/T = 1.2.

V_M [m/s]	T_{STB} [N]	T_{PS} [N]	T_T [N]	Q_{STB} [Nm]	Q_{PS} [Nm]	Q_T [Nm]	n_{STB} [1/s]	n_{PS} [1/s]	n_M [1/s]
0.480	3.49	3.05	6.54	0.039	0.035	0.074	9.72	9.73	9.72
0.690	6.58	5.63	12.21	0.074	0.065	0.139	13.52	13.52	13.52
0.759	8.29	6.82	15.11	0.094	0.081	0.175	14.96	14.96	14.96
0.900	13.27	11.10	24.37	0.148	0.131	0.279	18.71	18.72	18.72

Table 26: Results of self-propelled tests at DST d/L = 0.2, H/T = 1.2.

V_M [m/s]	Y_a [N]	Y_f [N]	Y [N]	N [Nm]
0.480	7.03	2.68	9.71	-8.38
0.690	16.34	6.77	23.11	-18.39
0.759	21.32	9.13	30.45	-23.41
0.900	48.91	22.70	71.61	-50.26

Table 27: Results of self-propelled tests at DST d/L = 0.1, H/T = 1.2.

V_M [m/s]	Fr [-]	Fr_h [-]	X_M [N]	P_{DM} [W]	z_{VM} [mm]	ϑ_M [1/60°]	φ [°]
0.479	0.053	0.299	-2.79	4.30	3.70	0.41	-0.039
0.690	0.076	0.430	-7.03	11.52	10.30	0.96	-0.082
0.759	0.076	0.430	-7.90	15.58	12.20	1.22	-0.094
0.900	0.099	0.560	-13.78	33.18	21.60	2.11	-0.153

the course of the test which is considered attributable to the moderate increase of propeller rates of revolution. In comparison to resistance tests in bare-hull condition, the bow-down trim of the model decreased with increasing forward speed due to the modified pressure field in the after body in response to the operating propellers, Fig. 14.

The results of propulsion experiments conducted in proximity to the tank wall are furnished with an additional table containing measured lateral forces, the integral lateral force and the yaw moment, Tables 23, 26 and 29. The propeller rate of revolution found from propulsion tests was used for each respective speed. The residual measured longitudinal force is F_{res}. No qualitative change in the trends was expected compared to towed resistance tests, but the effect of the operating propellers on the pressure field in the after body of the model ship is of interest. Fig. 15 shows the trends of midship sinkage and trim over forward speed and separation distance to the wall. Consistent with above mentioned theory and observations from towing tests, midship sinkage increased with decreasing distance to the tank wall. A significant observation was the decreasing bow-down trim angle the closer the model sailed to the wall in comparison to self-propelled tests in the centre of the tank. At the two smallest separation distances the model actually attained a bow-up trim. The blockage of the flow is assumed to reinforce the effect of the operating propeller on the pressure field in the after body, already observed in the results of tests in the centre of the tank. Moreover, the blockage of the flow leads to a more prominent wave crest between the bow and wall (see Tables 21, 24, 27).

Table 28: Results of self-propelled tests at DST d/L = 0.1, H/T = 1.2.

V_M [m/s]	T_{STB} [N]	T_{PS} [N]	T_T [N]	Q_{STB} [Nm]	Q_{PS} [Nm]	Q_T [Nm]	n_{STB} [1/s]	n_{PS} [1/s]	n_M [1/s]
0.480	3.16	3.00	6.16	0.036	0.035	0.071	9.74	9.74	9.74
0.690	6.24	5.44	11.67	0.073	0.063	0.136	13.55	13.55	13.55
0.759	7.72	6.77	14.49	0.088	0.078	0.176	14.96	14.97	14.97
0.900	13.41	12.09	25.50	0.147	0.136	0.283	18.69	18.70	18.70

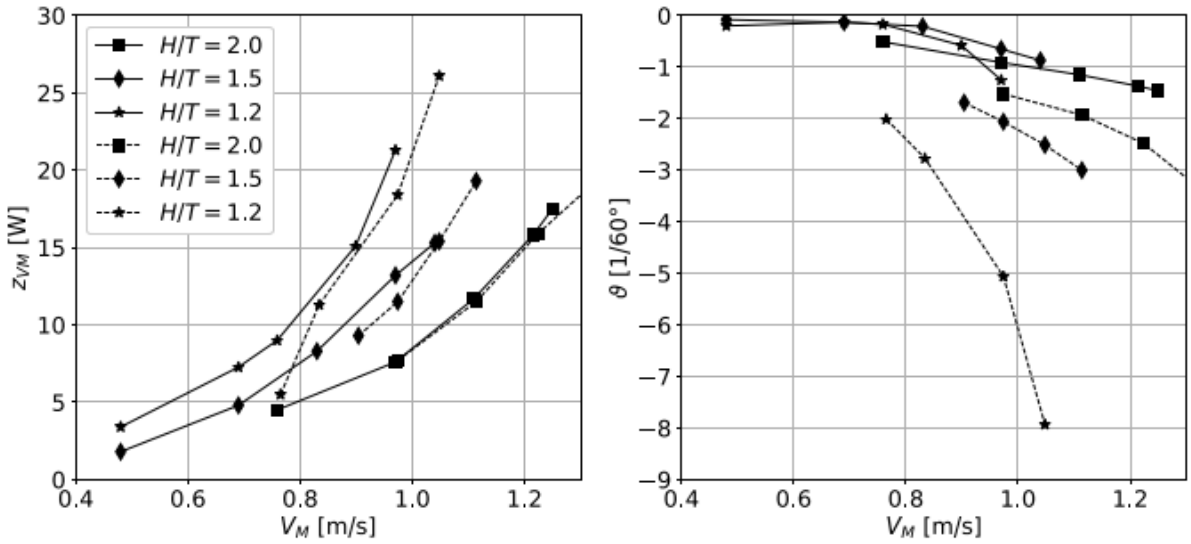

Figure 14: Sinkage (left) and trim angle (right) results over forward speed at different water depths. Full lines refer to the self-propelled model, dashed lines to the towed model.

Table 29: Results of self-propelled tests at DST d/L = 0.1, H/T = 1.2.

V_M [m/s]	Y_a [N]	Y_f [N]	Y [N]	N [Nm]
0.479	15.58	5.51	21.09	-19.38
0.690	33.86	14.87	48.43	-36.45
0.759	40.98	20.01	60.99	-40.18
0.900	77.81	47.35	125.16	-57.99

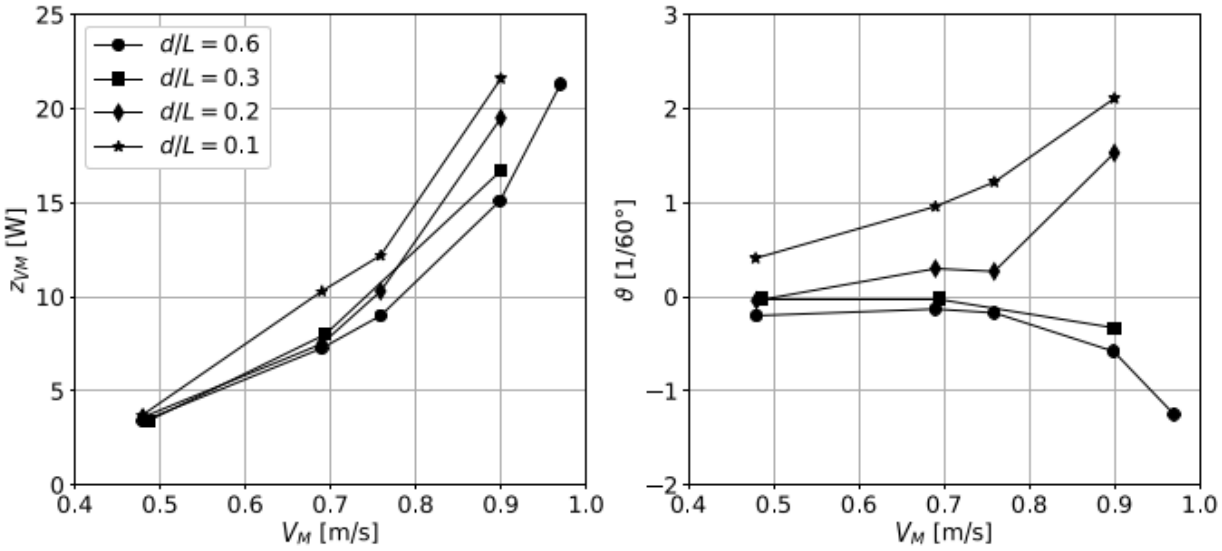

Figure 15: Sinkage (left) and trim angle (right) over forward speed and wall distance at H/T = 1.2. Full lines refer to the self-propelled model, dashed lines to the towed model.

The scrutiny of bank effects in sway and yaw modes of motions reveals that at the two closest separation distances to the wall both the suction force and yaw moment are generally and significantly greater in propulsion than in towing. Again, it was concluded that the operating propeller, in analogy to the change of squat between propulsion and towing, gives rise to a local decrease of the pressure ambient to the hull, thereby reinforcing the lateral suction force measured in the after body of the ship. (see Fig. 16)

4 Conclusions

Experimental results of resistance and propulsion tests with an inland waterway ship model at three water depths and three separation distances to a vertical wall at a fixed shallow water depth were generated to provide benchmark data for CFD. Hydrodynamic interactions between the model and flow restrictions related to squat and bank effects, as well as their impact on resistance and propulsion characteristics, were observed and quantified in experiments. Sensitivities to water depth and distance to the wall were found to be consistent with theory. In light of observed deviations of resistance predictions based on the solution of Reynolds-averaged Navier-Stokes (RANS) equations, Mucha et al. (2016), the presented set of experimental data may serve for comparison to numerical models using more elaborate turbulence modelling and the assessment of their reliability. Procedures for validation exercises can be found in Roach (1998), Ferziger and Peric (2002) or Larsson et al. (2013). A successfully validated and reliable numerical method may be used to vary test parameters and conditions and extend the available database for identification of coefficient-based mathematical models for manoeuvring taking into account the dependence on water-depth.

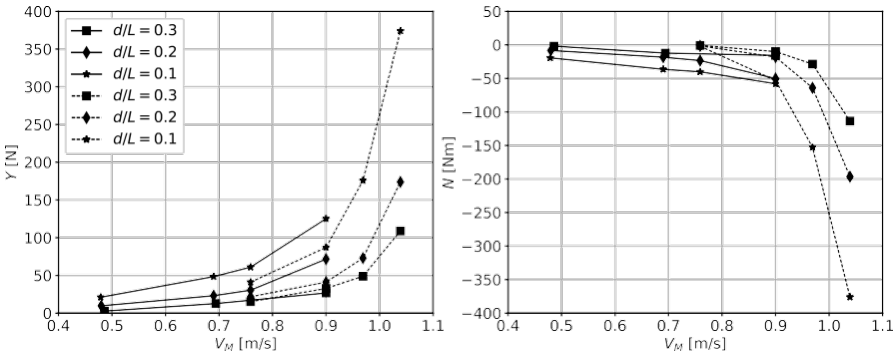

Figure 16: Suction force (left) and bow-out moment (right) over forward speed and wall distance at H/T = 1.2. Full lines refer to the self-propelled model, dashed lines to the towed model.

Funding

The work presented was funded by the Federal Waterways Engineering and Research Institute (Bundesanstalt für Wasserbau, BAW), Germany.

Acknowledgments

Results presented stem from a joint research effort of the Federal Waterways Engineering and Research Institute (Bundesanstalt für Wasserbau, BAW) and the Institute of Ship Technology, Ocean Engineering and Transport Systems (ISMT) of the University of Duisburg-Essen. Collaboration with Schiffbau Versuchsanstalt (SVA) Potsdam on the model-building and with DST on the design of the model, as well as on the conduction of experiments is acknowledged.

References

Bundestanstalt für Wasserbau, 2017. Inland Waterway Ship Test Case for Benchmarking. Available from: http://wiki.baw.de/en/index.php/Inland_Waterway_Ship_Test_Case.

Chen, X.N., 1999. Hydrodynamics of Wave-making in Shallow Water. PhD-Thesis. University of Stuttgart. Shaker Verlag.

Deng, G.B., Guilmineau, E., Leroyer, A., Queutey, P., Visonneau, M., Wackers, J., 2014. Simulation of a container ship in shallow water at model scale and full scale. In: Proc. Of the 3rd National CFD Workshop for Ship and Offshore Engineering.

Development Centre for Ship Technology, Transport Systems, 2014. Entwurf eines Referenzschiffes. DST Report 2112. (in German).

Eloot, K., Delefortrie, G., Vantorre, M., 2012. Inland navigation: assessing the manoeuvring behaviour for real-time simulation purposes. In: Proceedings of MARSIM 2012, pp. 1–12 Abstracts and Papers.

Eloot, K., Delefortrie, G., Vantorre, M., Quadvlieg, F., 2015. Validation of ship manoeuvring in shallow water through free-running tests. In: Proceedings of the 34th ASME International Conference on Ocean, Offshore and Arctic Engineering, OMAE2015-41912.

Ferziger, J., Peric, M., 2002. Computational Methods for Fluid Dynamics. Springer.

Graff, W., Kracht, A., Weinblum, G., 1964. Some extensions of D.W. Taylor's standard series. Trans. SNAME 72, 375–401.

Gronarz, A., 1997. Rechnerische Simulation der Schiffsbewegung beim Manövrieren unter besonderer Berücksichtigung der Abhängigkeit von der Wassertiefe. PhD-Thesis. Unversity of Duisburg (in German).

Jiang, T., 2003. Ship waves in shallow water. Fortschritt-Berichte VDI 13 (466).

Larsson, L., Stern, F., Visonneau, M., 2013. CFD in ship HydrodynamicsâResults of the gothenburg 2010 workshop. In: EÂ§a, L., Onate, E., Garcia-Espinosa, J., Kvamsdal, T., Bergan, P. (Eds.), MARINE 2011, IV International Conference on Computational Methods in Marine Engineering. Computational Methods in Applied Sciences, vol. 29 Springer, Dordrecht.

Lataire, E., 2014. Experiment-based Mathematical Modelling of Ship Bank Interaction. Ph.D. Thesis. University of Ghent.

Lataire, E., Vantorre, M., 2008. ship-bank interaction induced by irregular bank geometries. In: Proc. Of the 27th Symposium in Naval Hydrodynamics, Seoul, Korea.

Mucha, P., 2017. On Simulation-based Ship Maneuvering Prediction in Deep and Shallow Water. Ph.D. Thesis. University of Duisburg Essen.

Mucha, P., el Moctar, O., Böttner, C.U., 2015. Technical note: PreSquat - workshop on numerical prediction of ship squat in restricted waters. Ship Technology Research - Schiffstechnik 61 (3), 162–165.

Mucha, P., Deng, G., Gourlay, T., el Moctar, O., 2016. Validation studies on numerical prediction of ship squat and resistance in shallow water. In: Proc. Of the 4th International Conference on Ship Manoeuvring in Shallow and Confined Water with Special Focus on Ship Bottom Interaction.

Mucha, P., el Moctar, O., Dettmann, T., Tenzer, M., 2017. Inland waterway ship test case for resistance and propulsion prediction in shallow water. Ship Technol. Res. 64 (2), 106–113.

Roache, P.J., 1988. Verification of codes and calculations. AIAA J. 36 (No. 5), 696–702 (1998).

Terziev, M., Tezdogan, T., Oguz, E., Gourlay, T., Demirel, Y.K., Incecik, A., 2018. Numerical investigation of the behaviour and performance of ships advancing through restricted shallow waters. J. Fluid Struct. 76, 185–215.

The International Towing Tank Conference, 1999. 1978 ITTC Performance Prediction Method 7.5-02-03-01.4. Available from: http://ittc.info.

Thomas, B., Sclavounos, P.D., 2006. Optimal Control Theory Applied to Ship Maneuvering in Restricted Waters, Readings in Marine Hydrodynamics. (Volume to be Published in Honor of Professor J. Nicholas Newman).

Tonelli, R., Quadvlieg, F., 2015. New Benchmark Data for Manoeuvring in Shallow Water Based on Free Running Manouevring Tests Including Uncertainty of the Results Proceedings of the ASME. OMAE Paper No. 42254.

Tuck, E.O., 1978. Hydrodynamic problems of ships in restricted waters. Annu. Rev. Fluid Mech. 10, 33–46.

Vantorre, M., Verzhbitskaya, E., Laforce, E., 2002. Model test based formulations of ship-ship interaction. Schiffstechnik 49, 124–141.

Authors

Philipp Mucha
Federal Waterways Engineering and Research Institute (BAW),
Kußmaulstraße 17, 76187 Karlsruhe, Germany
E-Mail: philipp.mucha@baw.de

Ould el Moctar
University of Duisburg-Essen, Forsthausweg 2, 47057 Duisburg, Germany

Thorsten Dettmann
Federal Waterways Engineering and Research Institute (BAW),
Kußmaulstraße 17, 76187 Karlsruhe, Germany

Matthias Tenzer
Development Centre for Ship Technology and Transport Systems (DST), Oststraße 77,
47057 Duisburg, Germany